Ionic Conductivity of Doped Lanthanum Gallate and Strontium Gallate Composites

ECS Transactions, 80 (9) 141-149 (2017)
10.1149/08009.0141ecst ©The Electrochemical Society

Ionic Conductivity of Doped Lanthanum Gallate and Strontium Gallate Composites

S. L. Reis and E. N. S. Muccillo

Energy and Nuclear Research Institute – IPEN, Av. Prof. Lineu Prestes, 2242
Cidade Universitária, S. Paulo, 05508-000, SP, Brazil

Polycrystalline ceramic solid electrolytes based on strontium- and magnesium-doped lanthanum gallate exhibit high ionic conductivity and find potential application in solid oxide fuel cells operating at intermediate temperatures. Sintering of this solid electrolyte is usually carried out at high temperatures, being responsible for loss of Ga and consequent formation of impurity phases. In this work, composites consisting of $La_{0.9}Sr_{0.1}Ga_{0.8}Mg_{0.2}O_{3-\delta}$ with additions of strontium gallate were prepared by solid state reaction, and the influence of the additive on electrical conductivity and phase composition of the composite electrolyte was investigated. The sintered density of composites is higher than 95% of the theoretical value after sintering at 1350°C. The contents of impurity phases decreased with increasing additions of strontium gallate. The overall ionic conductivity of the composites is higher than that of LSGM. This effect is attributed to the decrease in the fraction of free MgO at grain boundaries in the composites.

Introduction

Lanthanum gallate with partial substitutions by strontium and magnesium in the A- and B-sites, respectively, $La_{1-x}Sr_xGa_{1-y}Mg_yO_{3-\delta}$ are good oxide-ion conductors and potential candidates for application in Solid Oxide Fuel Cells (SOFCs) operating at intermediate temperatures (~500-700°C) (1). In addition to the high ionic conductivity, these solid electrolytes exhibit low electronic conductivity and wide range of chemical stability (1,2). The main constraint regarding this solid electrolyte with perovskite structure, for application in SOFCs, is related to impurity phases.

The impurity phases reported in doped lanthanum gallate are $LaSrGaO_4$, $LaSrGa_3O_7$, $La_4Ga_2O_9$, and MgO (1,2). In general, the relative fractions of these phases are low, such that for compounds prepared by chemical methods, they are barely detected by conventional X-ray diffraction (3,4). Moreover, it has been already shown that these impurity phases may not be detected on the outer surface of sintered specimens (5). Among the most frequently investigated compounds within this family the one with stoichiometry $La_{0.9}Sr_{0.1}Ga_{0.8}Mg_{0.2}O_{3-\delta}$, hereafter LSGM, exhibits the lowest fraction of impurity phases (6).

$LaSrGaO_4$ and $La_4Ga_2O_9$ phases display low ionic conductivity (~ 10^{-4} and ~ 10^{-5} $S.cm^{-1}$, respectively at 800ºC), whereas MgO and the stoichiometric $LaSrGa_3O_7$ are insulating phases (6). The relative fractions of impurity phases depend on several factors,

such as temperature/time profile during sintering and relative amounts of the constituent oxides.

Recently, composite electrolytes have been investigated as alternative materials for SOFCs taking advantage of specific properties of every component. Most of reported studies involve well-known solid electrolytes as yttria-stabilized zirconia, doped-ceria and doped lanthanum gallate (7-9). In these previous studies, improvement of the electrical or mechanical properties is claimed.

In this work, the effect of addition of strontium gallate, SG, to LSGM is investigated. It has already been shown that SG improved the densification of yttria-stabilized zirconia and gadolinia-doped ceria by forming liquid phase during sintering (10,11). Results of ionic conductivity of the composite electrolyte are explained taking into account the final microstructure.

Experimental

Composites of $La_{0.9}Sr_{0.1}Ga_{0.8}Mg_{0.2}O_{3-\delta}$ and strontium gallate were prepared by mixing the starting oxides followed by high temperature reaction. The starting powders were La_2O_3 (99.9%), Ga_2O_3 (99.99%) and reagent grades MgO and $SrCO_3$. At first, the lanthanum powder was thermally treated at 1000°C for 3 h. $La_{0.9}Sr_{0.1}Ga_{0.8}Mg_{0.2}O_{3-\delta}$ was prepared by calcination of the starting materials at 1250°C for 12 h with intermediate grindings followed by attrition milling for 1 h with zirconia media in alcoholic medium. SG powder was obtained from mixture of dried $SrCO_3$ and Ga_2O_3. The mixed powder was attrition milled for 1 h and calcined at 1200°C for 1 h. The prepared composites of LSGM/SG contained 0.5, 1.0 and 1.5 mol% SG.

Cylindrical specimens were obtained by uniaxial and cold isostatic pressing (100 MPa). The green compacts were sintered at 1350°C for 0.5 and 5 h with 5°C.min^{-1} heating rate.

Characterization of sintered specimens was carried out by X-ray diffraction, XRD (Bruker-AXS, D8 Advance), in the $20^o \leq 2\theta \leq 80^o$ range. The sintered density was determined by the immersion method using distilled water. The microstructure of polished and thermally etched surfaces was observed by field emission gun scanning electron microscopy, FEG-SEM (FEI, Inspect F50). The mean grain size was estimated by the intercept method (12). The ionic conductivity was evaluated by impedance spectroscopy measurements (HP 4192A), with 100 mV of applied AC voltage in the 5 Hz to 13 MHz and 280-420°C frequency and temperature ranges, respectively. Silver paste was applied onto large surface of specimens and cured at 400°C to act as electrode. Data were collected in impedance mode and analyzed by specific software (13).

Results and Discussion

Figure 1 shows X-ray diffraction patterns of SG powders after attrition milling and after calcination at 1200°C for 1 h. The main XRD reflections after milling are ascribed to those characteristics of the starting oxides and with $Sr_3Ga_4O_9$ phase. After calcination the

XRD pattern exhibits the typical reflections of $Sr_3Ga_2O_6$ phase with $Sr_3Ga_4O_9$ as minor constituent.

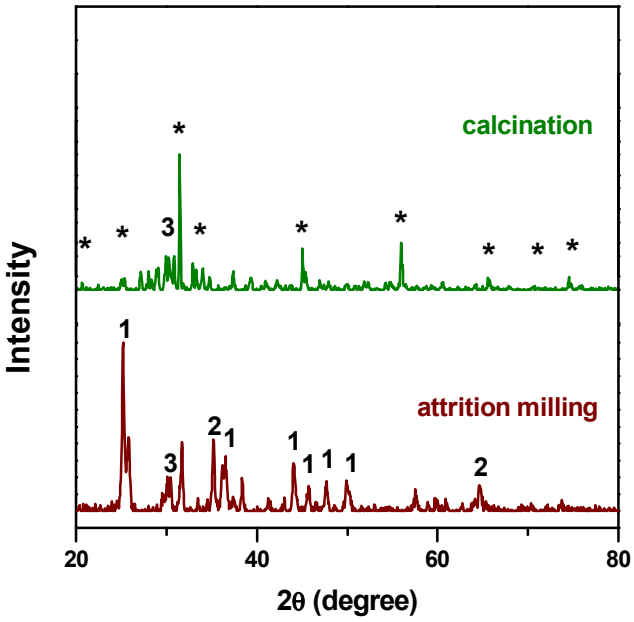

Figure 1. Powder XRD patterns of the mixture of $SrCO_3$ and Ga_2O_3 before and after calcination at 1200°C for 1 h. 1-$SrCO_3$, 2-Ga_2O_3, 3-$Sr_3Ga_4O_9$ and * $Sr_3Ga_2O_6$.

Figure 2 shows FEG-SEM micrographs of SG powders after (a) attrition milling and (b) calcination at 1250°C for 1 h. The morphology of powder particles is uniform after milling with few agglomerates. The calcined powder consists of small SG grains.

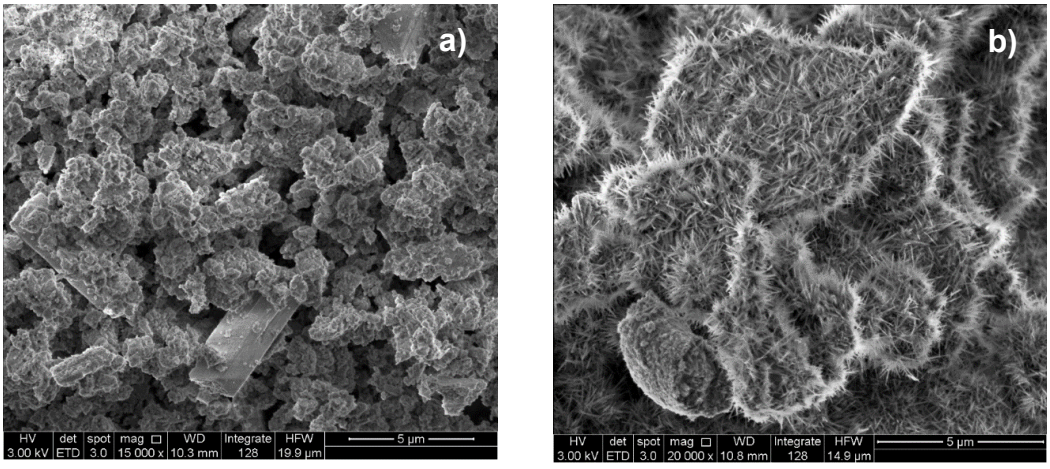

Figure 2. FEG-SEM micrographs of SG powder mixture after (a) attrition milling and (b) calcination at 1200°C for 1 h.

Figure 3 depicts XRD patterns of LSGM and LSGM/SG composites sintered at 1350°C for (a) 0.5 and (b) 5 h. In this figure, the right-hand pattern displays a zoomed

view of the 25-32º angular range, where the most intense peaks of the impurity phases are recorded. All specimens exhibit the characteristic reflections of the orthorhombic phase (indicated by *) along with very small intensity peaks of $LaSrGaO_4$ and $La_4Ga_2O_9$ phases (indicated by 1 and 2, respectively). The amount of impurity phases has not been quantified, but the XRD patterns were normalized for the most intense reflection of the orthorhombic phase for comparison purpose. It may be seen that the contents of impurity phases decrease with increasing sintering time.

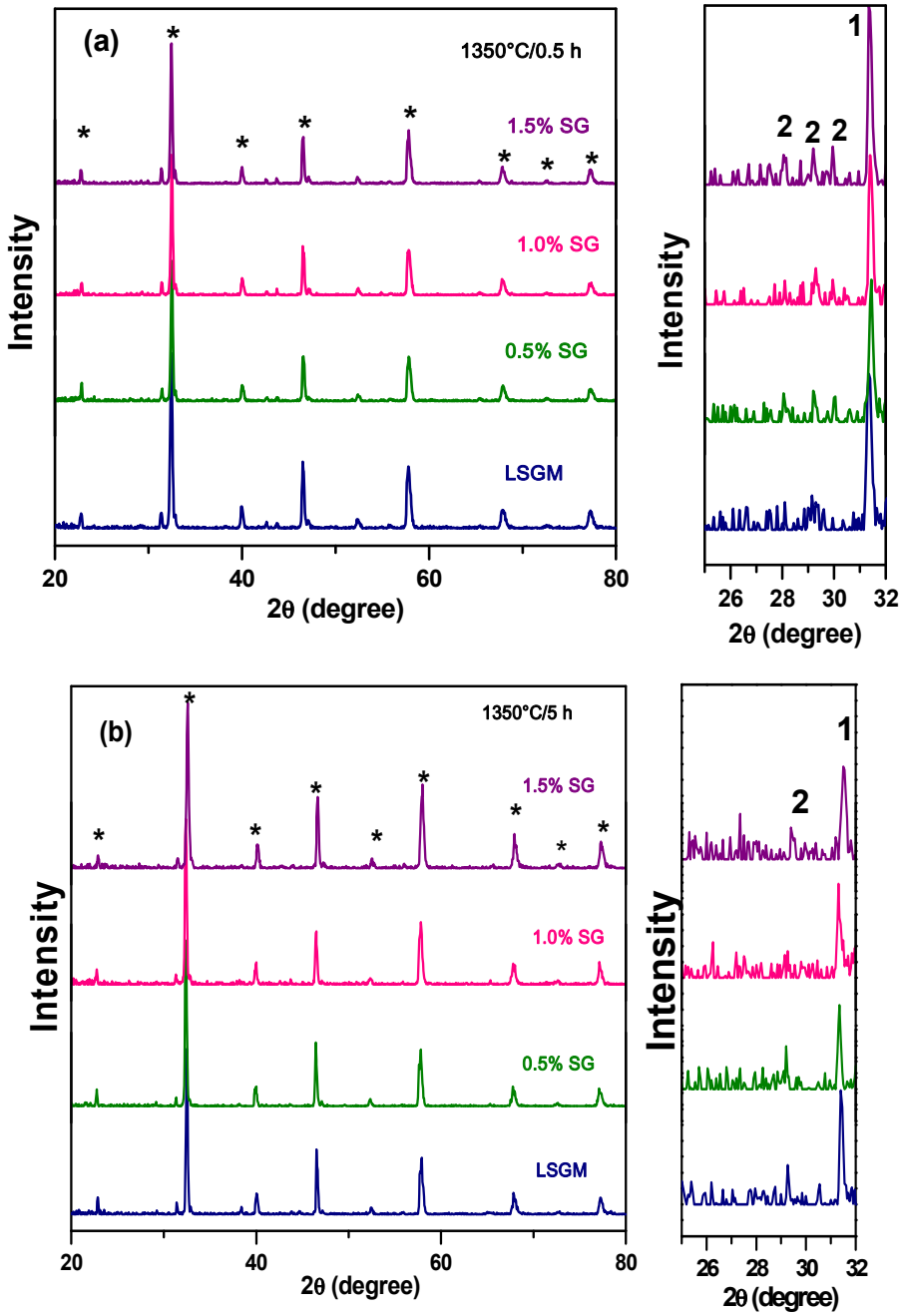

Figure 3. XRD patterns of LSGM and LSGM/SG composites after sintering at 1350°C for (a) 0.5 and (b) 5 h. Right-hand patters are a zoomed view of the 25-32º angular range. (*) LSGM, (1) $LaSrGaO_4$, (2) $La_4Ga_2O_9$.

Typical microstructure features of LSGM and LSGM/SG composites for specimens sintered at 1350°C for 5 h are shown in the representative FEG-SEM micrographs of Figure 4. The microstructure of LSGM (Figure 4a) is heterogeneous with grain size in the micrometer range and several nanosized dark grains at the grain boundaries. These nanosized grains correspond to free MgO (3,14). The microstructure of LSGM/SG composites is exemplified in Figure 4b for the specimen containing 1.5 mol% SG. Surprisingly, the composite shows more homogeneous microstructure with reduced number of nanosized MgO grains. This result suggests that strontium gallate acts at the interfaces of LSGM grains during sintering, most likely by changing the interface energy, and preventing ex-solution of MgO from LSGM and further migration to the grain boundaries.

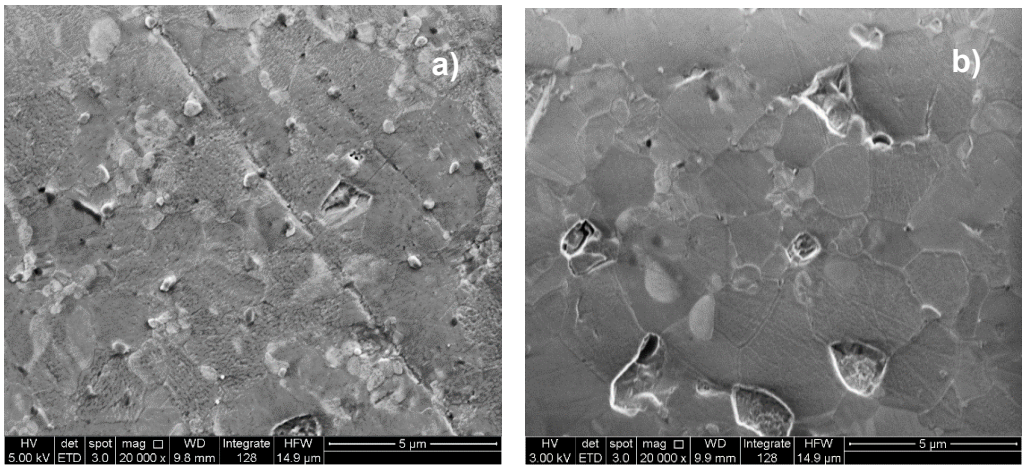

Figure 4. FEG-SEM micrographs of (a) LSGM and (b) LSGM/SG composite with 1.5 mol% SG. Sintering: 1350°C for 5 h.

Table I lists values of relative density of sintered composites. The density is high (above 95% of the theoretical value) and seems to be independent on the fraction of SG. In this calculation 6.67 $g.cm^{-3}$ was taken as theoretical density (ICSD 51-288, $La_{0.9}Sr_{0.1}Ga_{0.8}Mg_{0.2}O_{3-\delta}$). The mean grain size slightly decreases with increasing the fraction of SG in the composite. Then, strontium gallate acts also as a grain growth inhibitor for LSGM.

Table I. Values of Sintered Density and Mean Grain Size of LSGM and LSGM/SG Composites According to the Sintering Profile.

% SG	Temperature/time (°C /h)	Relative Density (%)	Mean grain size (µm)
LSGM	1350/0.5	97.2	1.64 ± 0.05
0.5	1350/0.5	96.6	1.34 ± 0.03
1.0	1350/0.5	95.8	1.23 ± 0.02
1.5	1350/0.5	95.5	1.15 ± 0.03
LSGM	1350/5	98.5	2.93 ± 0.07
0.5	1350/5	98.0	2.67 ± 0.08
1.0	1350/5	97.1	2.64 ± 0.08
1.5	1350/5	96.6	2.40 ± 0.07

Impedance spectroscopy diagrams of specimens sintered at 1350°C for (a) 0.5 and (b) 5 h are depicted in Figures 5a and 5b, respectively. In these plots the impedance was normalized for specimen dimensions and numbers over experimental data are the decimal logarithm of frequency (in Hz). The shape of these spectra is similar and does not depend on the sintering profile or the fraction of SG in the composite. However, for specimens sintered for 5 h (Figure 5b), the grain boundary contribution to the total electrical conductivity is negligible. Thus, in this case, only the grain conductivity was evaluated.

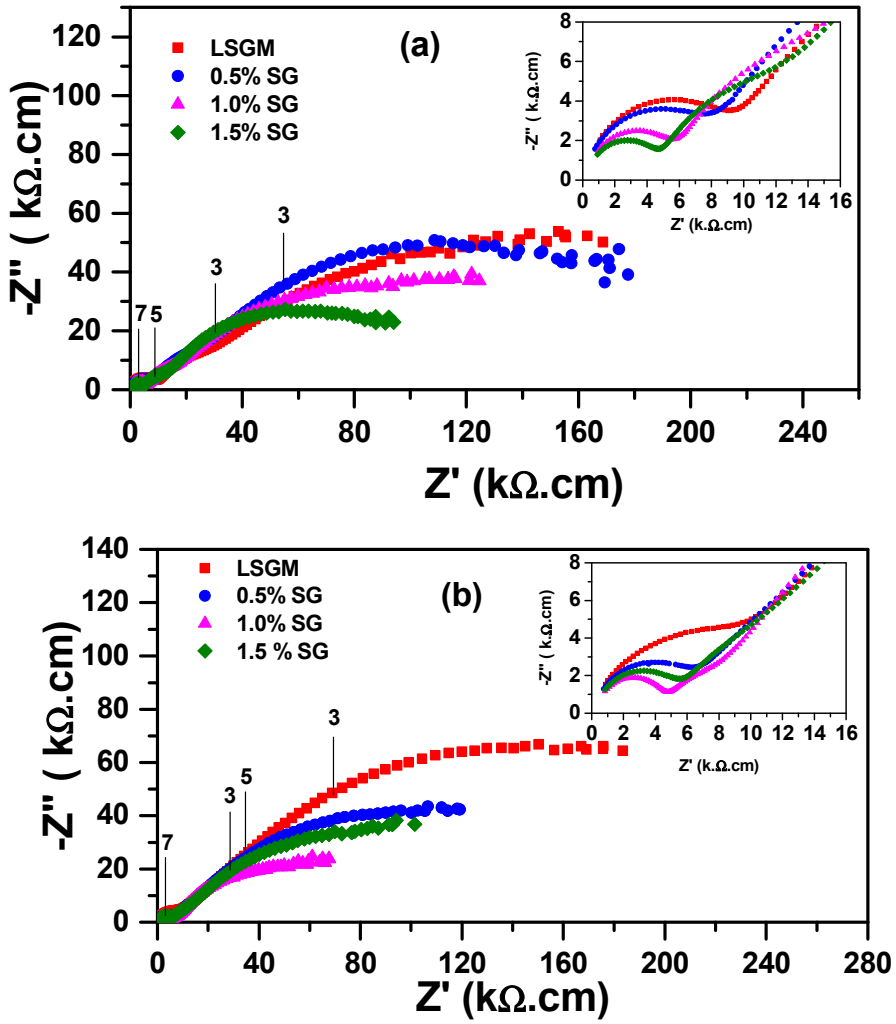

Figure 5. Impedance spectroscopy diagrams of LSGM and LSGM/SG composites sintered at 1350°C for (a) 0.5 and (b) 5 h. Temperature of measurement: 355°C.

Figure 6 shows Arrhenius plots of the (a) grain and (b) grain boundaries for LSGM and LSGM/SG sintered for 0.5 h at 1350°C. In general the grain and grain boundary conductivities increase with increasing the SG fraction in the composite electrolyte.

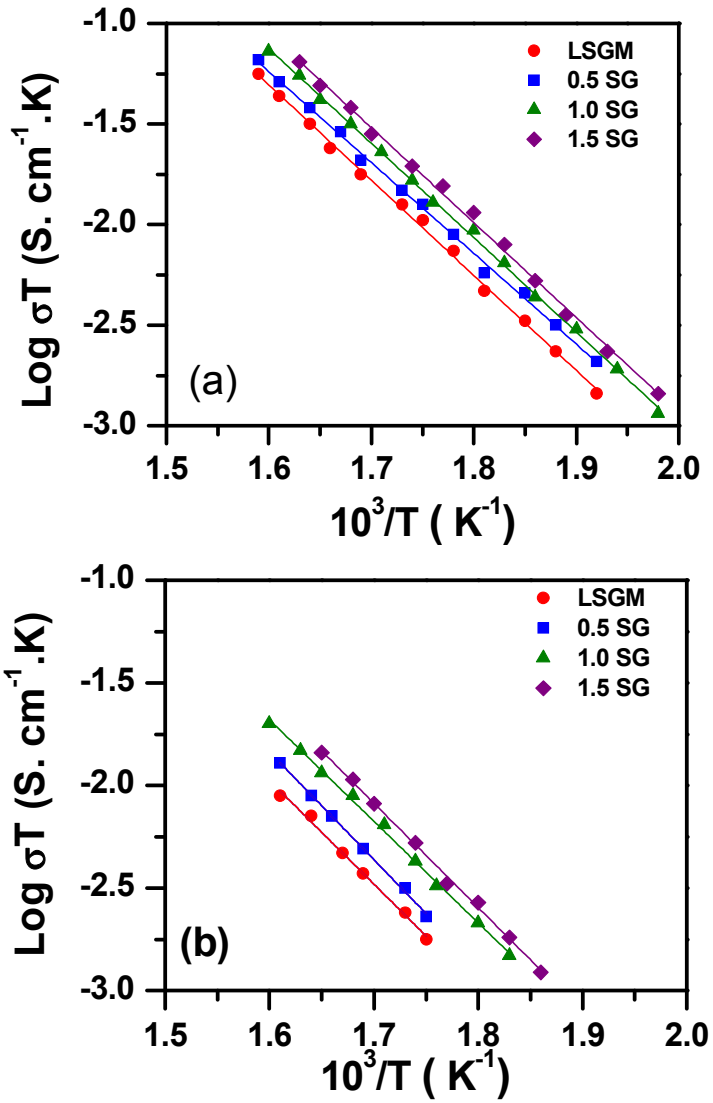

Figure 6. Arrhenius plots of the (a) grain and (b) grain boundary conductivities of LSGM and LSGM/SG composites sintered at 1350°C for 0.5 h.

The same effect is observed for the grain conductivity of specimens sintered for 5 h (Figure 7).

The enhanced ionic conductivity of LSGM/SG composites compared to LSGM may be ascribed to the beneficial effect of SG avoiding migration of MgO towards the grain boundaries and formation of LSGM grains with depleted magnesium concentration, in general agreement with microstructure features.

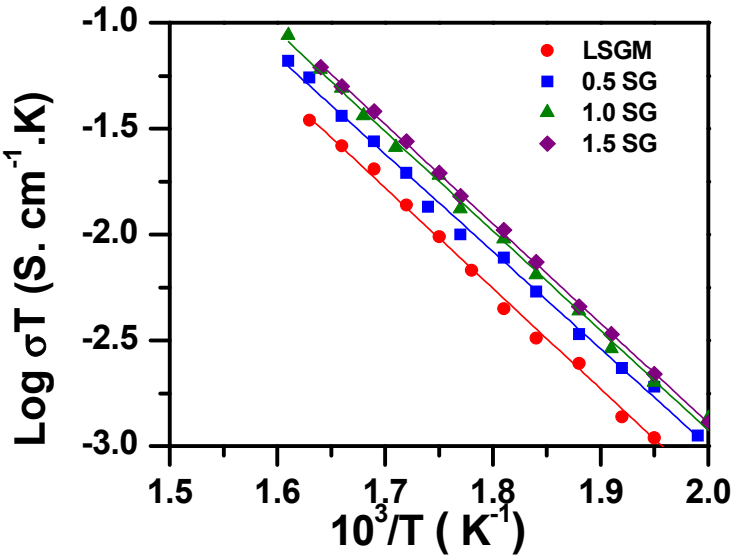

Figure 7. Arrhenius plots of the grain conductivity of LSGM and LSGM/SG composites sintered at 1350°C for 5 h.

Conclusions

Composites consisting of LSGM and SG were prepared by solid state reactions. The sintered density of composites is high (>95% of the theoretical value) after sintering at 1350°C. The fraction of common impurity phases in LSGM decreases with addition of strontium gallate and with increasing the sintering dwell time. SG inhibits the grain growth of LSGM and reduces the fraction of free MgO at grain boundaries. The grain and grain boundary conductivities of LSGM/SG composites is higher than those of LSGM.

Acknowledgments

To FAPESP (Proc. 2013/07296-2), CNPq (Proc. 304073/2014-8 and 505980/2013-4) and CNEN for financial supports.

References

1. T. Ishihara, M. Honda and Y. Takita, *J. Am. Ceram. Soc*., **116**, 3801 (1994).
2. M. Feng and J.B. Goodenough, *Eur. J. Solid State Inorg. Chem*., **31**, 663 (1994).
3. R. Polini, A. Pamio and E. Traversa, *J. Eur. Ceram. Soc*., **24**, 1365 (2004).
4. S.L. Reis and E.N.S. Muccillo, *Adv. Mater Res*., **975**, 81 (2014).
5. E. Djurado and M. Labeu, *J. Eur. Ceram. Soc*., **18**, 1397 (1998).
6. M. Rozumek, P. Majewski, F. Aldinger, K. Künstler and G. Tomandl, *CFI-Ceramic Forum Int./Ber. D. Keram. Ges*., **80**, E35 (2003).
7. B. Li, S.F. Liu, X.M. Liu, G.Y. Hao, H.P. Wan and W.H. Su, *Int. J. Hydrogen Energy*, **38**, 11392 (2013).
8. R.K. Singh Raghvendra and P. Singh, *J. Mater. Sci*., **49**, 5571 (2014).

9. Y.C. Wu, M.J. Lee and X. Li, *J. Eur. Ceram. Soc*., **35**, 4485 (2015).
10. M. Feng and J.B. Goodenough, *J. Am. Ceram. Soc*., **77**, 1954 (1994).
11. J.-S. Lee, *J. Electroceram*., **17**, 709 (2006).
12. M.J. Mendelson, *J. Am. Ceram. Soc*., **52**, 443 (1969).
13. M. Kleitz and J.H. Kennedy, *Fast Ion Transport in Solids, Electrodes and Electrolytes*, P. Vashishta, J. N. Mundy and G. K. Shenoy, Editors, p. 1858, North-Holland, Amsterdam (1979).
14. S.L. Reis and E.N.S. Muccillo, *Ceram. Int*., **42**, 7270 (2016).